Project	ICESTARS
Project Number	FP72008ICT214911
Work Package	WP3
Tasks	T3.4
Deliverable	D3.7 - version 1.0

title	Public Report on EM Field Solving within Circuit Simulation, Optimization of Device Design based on RF Boundary Conditions and Reference Benchmarks For Mixed-Signal Design
authors	Sascha Baumanns, Michael Matthes Caren Tischendorf, Monica Selva Soto Wim Schoenmaker*, Peter Meuris , Gabor Bella Bart De Smedt, Wim Verhaegen Rick Janssen
Affiliations	University of Cologne MAGWEL NV NXP Semiconductors
*** corresponding author**	wim.schoenmaker@magwel.com
date	September 30 , 2010

Contents

1 Abstract

This document is an executive summary of the activities within the ICESTARS project's work package 3. The document gives an overview of the detailed activities during the project runtime with specific emphasis on the development decisions that were taken when performing the tasks in the work package 3, entitled "EM Analysis and Coupled EM-Circuit Analysis".

2 Introduction

When entering new regions in the frequency spectrum or when devices are required with faster temporal response, one can only construct reliable integrated circuits if the underlying models for the devices that are submitted to integration are accurately covering the newly entered regions. For the ICESTARS project, the goal has been to produce accurate models for designs in the 60 GHz range. It is a common phenomenon that at fast switching times and at higher frequencies, devices experience each other's presence by exchanging energy through electromagnetic radiation. Whereas, this effect is exploited in communication devices (antennas) it can also be a so-called parasitic effect that will deteriorate the proper operation of circuits if such effects have not been included in the lay-out and accounted for. Thus a key question in modeling at unexplored frequency ranges is whether the models are sufficiently detailed to deal with such radiation effects. In order to address this question, it is demanded that early-stage model verification is possible. The device models that are used for designed complex integrated circuits are very 'compact', i.e. using a limited set of variables one attempts to grasp the dynamical behavior of the devices for a wide variety of conditions. The derivation of these 'compact models' is a science (and art) by itself and requires skills in physical reasoning, mathematics and knowledge of the forecasted applications. An important aid in this process is the use of tools that mimic the more detailed physics that participates in the response of the devices as well as the interaction between the devices. The detailed physics is captured in the famous so-called Maxwell equations that provide a full account for the electromagnetic fields. Yet, the Maxwell equations are not sufficient. They allow us to predict the fine details of the electromagnetic fields provided that we know the space-time distribution of the charges and current densities. A second set of equations is needed to determine the latter. The so-called constitutive relations inform us about the charge and current densities, provided that we know how the electromagnetic fields look like. For example, the most well-known constitutive relation is Ohm's law which simply states that the current density is proportional the electric field intensity and the constant of proportionality is the conductance. Thus, we are locked into a 'catch 22' scenario: In order to compute the electromagnetic fields one must know the charge-current densities, and in order to compute the latter, one must know the electromagnetic fields. The way out of this scenario is to start from Maxwell's equations and substitute right at the start the constitutive relations for the charge and current densities. The result is a highly non-trivial set of equations whose solution can often only be obtained by numerical means. Taking into account that the solutions will depend on the boundary conditions and that the boundary conditions depend on the application, it is evident that the construction of a solution method is a serious effort. Moreover, the so-called 'constants' (e.g. conductivity) are in reality not constant at all but may themselves depend on field intensities. A big part of the work performed in work package 3 of the ICESTARS project was devoted to provide a substantial contribution to the solution method on the above described problem (the field solver).

Even after having found a solution method for the problem as described above, one can not skip the use of the compact models. The main reason is that the field solving solution methods are very computationally intensive. In general it is advised to restrict the use of the field solving in IC design to restricted domains and for the remainder exploit the compact models. Thus it becomes interesting to combine the field solver directly with the compact-model based solver (the circuit simulator). To be more precise, given a complete lay-out: can one solve the bulk of the lay-out using compact models and circuit simulation and split off a small part by the much more computational intensive field simulation? Again a little reflection shows that this leads again to a catch 22 or self-consistency scenario. In order to set the boundary conditions for the field solver, one must know which currents and voltages are provided by the circuit, but in order to know the latter, one must know, which currents and voltage are to be expected from

the field solution. A second big part of the work performed in work package 3 of the ICESTARS project was devoted to provide a substantial contribution to the solution method to solve this self-consistency problem.
Being equipped with an answer to above self-consistency problems we can realize the objectives of workpackage 3. These objectives are:

- To characterize and optimize functional devices taking into account the electromagnetic interaction between neighboring devices
- To extract compact RF models of the devices suitable for reduced-order modeling
- To give accurate transient characterization of devices and elementary combinations thereof by identifying preferred paths of energy propagation
- To contribute to a profound understanding of mixed-signal design by creating a collection of benchmarks that may serve as references by using EM simulations and measurements.

When defining the tasks in work package 3, we followed a three-stage approach, based on the following ingredients:

- Which background knowledge and tools are available to achieve the objectives of the work package?
- Starting from this background which tasks need to be performed to achieve the objectives?
- What are appropriate test cases for guiding the development activities?

In particular, the last item is of key importance. Software development remains a futile effort without intensive testing. It is interesting to note that in the testing phase, Pareto's law seems to be remarkably well respected: Removing the last 10% of the causes for failures consumes 90% of the effort. While developing the software tools in Tasks T3.2 and T3.3, we can only confirm this observation. Therefore, it really makes sense to report on the gathered experience during the development of the software such that valuable recommendations can be extracted for future projects. Moreover, it also allows the users of the software to esteem its intrinsic quality and validity of the numerical results that are produced.
This document is divided in several chapters which can be read more or less independently. Each chapter describes a specific test path and the paths are rather independent. One will find a rather accurate mapping of the activities described in the description of work on the chapters in this document.

3 Background knowledge and tools

The available back ground knowledge in the ICESTARS project is based on the availability of a electromagnetic field solver in the frequency regime that possesses the unique feature of dealing with semiconducting materials as is. Whereas there are several electromagnetic field solvers at the market, they all consider semiconductors as some moderately conducting metal with a rather large permittivity. Such an approximation ignores the fact that the currents in semiconductors can consists both of positively charged holes and negatively charged electrons. MAGWEL has developed a tool that is released from this approximation, but it requires that the field equations are described in terms of 'potentials'. Whereas many electromagnetic field solvers address the field directly their basic variables refer to *forces*. On the other hand the potentials refer to *energy* and the latter is an essential parameter for computing the number of holes and electrons in a semiconductor accurately [1].

At the university of Cologne, the mathematics department has extensive background knowledge of implicit and adaptive time integration. This knowledge was already applied to circuit simulation. Bringing together the knowledge of Cologne and MAGWEL, the gaps could be filled to construct a field solver that 'speaks the language of a circuit simulator' , i.e. a field solver that operates in the transient (time) regime and moreover, the circuit simulator can be extended to include a field solver part such that the self consistency is sustained. Finally, NXP as a third contributor in the work package brings in the knowledge about industrial relevant test structures, benchmarking and testing as well as defining the user interface of the newly tool suite.
It should be noted that the MAGWEL field solver is developed much more recently than many of the existing field solvers that are around already for more than two decades. As a consequence, it was needed to confirm that the solution method based on potentials really is sufficiently mature in order to deal with the advanced structures that are found in the integrated circuits, e.g. building elements of low-noise amplifiers (LNAs) and voltage controlled oscillators (VCOs). For that purpose a task was included to perform the simulations of a series of selected devices using third party tools as well as the MAGWEL field solver. The outcome of the task was that the solution method based on potentials is equally capable of dealing with these structures. On the positive side it is concluded that the method is more easily integrated into circuit simulators because the boundary conditions refer to the same variables, i.e. voltages at nodes and currents in links (branches). On the negative side, the solver requires further development for adaptive meshing. The adaptive meshing method was initiated in the project but is not yet complete. This is partly due to the fact that the only more or less robust adaptive meshing strategies are based on tetrahedron cells mesh generators. These mesh elements are not necessarily the best choice for microelectronic applications, because for microelectronic structures one is confronted with structures with distorted scales. Many orders of magnitude variations of typical sizes are found in a design. In other words, for the simulation of a single structure one encounters details in the nanometer range co-existing with patterns in the hundreds of micron range. The MAGWEL solver has addressed this aspect by constructed mesh generation facilities that take care of this aspect. However, it also has as a consequence that adaptive meshing needs to be reconsidered for other cell configuration as the tetrahedron. Another and more severe concern of the potential solution method is that an important class of solvers, being the iterative ones such as GMRES, BiCGSTAB experience more difficulty in finding the solution when the frequency increases. Typically, above 50 GHz the number of iterations that is needed to find the solution increases dramatically. An in-depth analysis of this problem was done and it was found that the condition number of the corresponding linear system, which is a measure for 'ease of solving' increases. This problem is not new and it is already known for the conventional field solvers. However, what is new is that here it is encountered in the high-frequency regime (the ultraviolet catastrophe) whereas for the conventional field solvers it is found at zero Hertz frequency (infrared singularity). As a solution to this problem we have proposed a variable transformation such that at all circumstances the low and high frequency collapse can be avoided.

4 RF Boundary conditions

The RF boundary conditions have been part of the development work. Originally, the MAGWEL field solver was designed as a refinement of a technology computer-aided design (TCAD) tool. Therefore, the boundary conditions were set up in such a way that when applying the tool to some device architecture, the simulation boundaries were equiped with field configurations, such that the interior is electrically neutral and no electric field is found perpendicular to the boundary and moreover, only tangential magnetic field are found which come with the load wires of the contact areas. However, at high frequency such energetic closure becomes doubtful

and one must allow for the possibility that energy can leave or enter the simulation through a boundary where no metallic contact is found. Such radiation boundary conditions are already known in finite-difference time domain simulation, but have not been addressed for a field solver in which the potentials are the starting variables. This problem has been addressed as one of the activities in this work package. We have been able to identify and classify various boundary conditions. The old TCAD-like boundary conditions can be seen as Dirichlet boundary conditions for the potentials, whereas the radiative boundary conditions take the appearance of Neumann boundary conditions. One should be aware of the fact that the boundary conditions must be chosen for the scalar potential as well as for the vector potential. Whatever one chooses, in the end the choice should be compatible with the gauge condition that is imposed to make the solution unique everywhere. Once having performed a detailed analysis of these issues we have applied the radiative boundary conditions in the potential formulation for boundaries where we expect free waves leaving the simulation domain.
As is seen in Fig. 1, the magnetic field is not dropping to zero when the boundary of the simulation domain is reached.

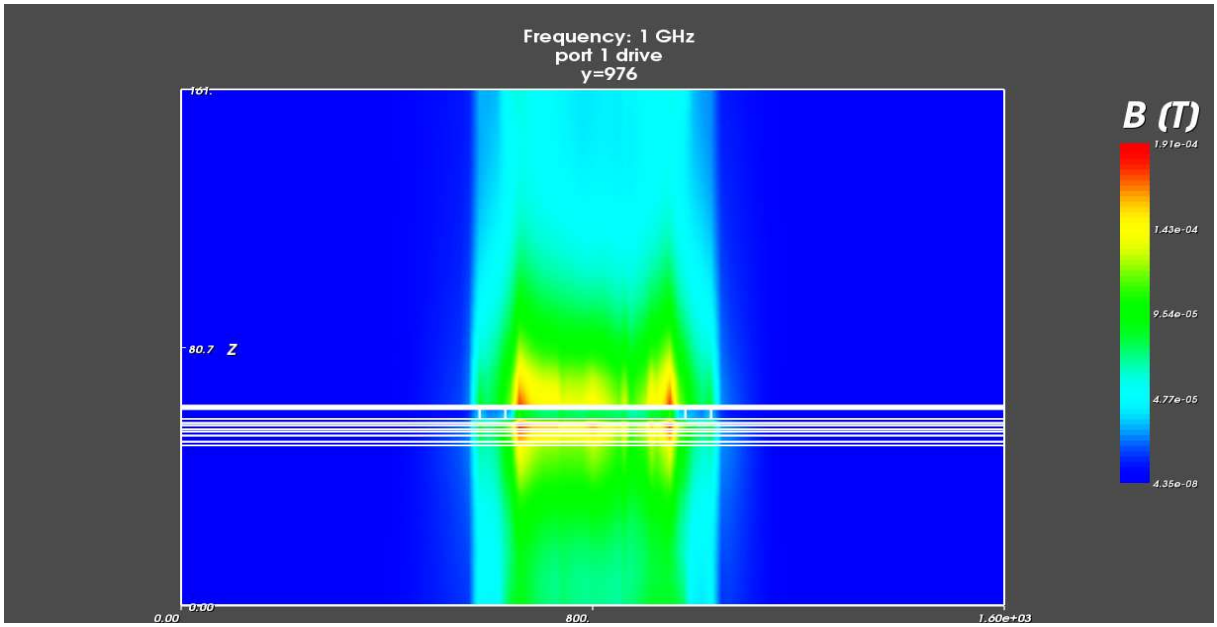

Figure 1: Magnetic induction at 1GHz radiating out of the spiral inductor. With RF boundary condition the field differs from zero at the edge (top/bottom) of the simulation domain.

In order to appreciate the problem, let us describe the paradox that pops up when a detailed analysis is made of the experimental set up. The basic question is: "Where is the ground?" An experimental set up consists of attaching probes to the signal pads on the test structure. A clear illustration of the set up is shown in Fig. 2. The outer conductors (shields) of the coax cables are connected to a common ground in the VNA (Vector Network Analyzer). For a symmetric set up, we may expect this common ground is also found at the left and right ground pads of the device under test.

In general the theoretical analysis of the coax wires leads to two important observations:

- The current on the inner wire is equal and opposite to the current on the shield

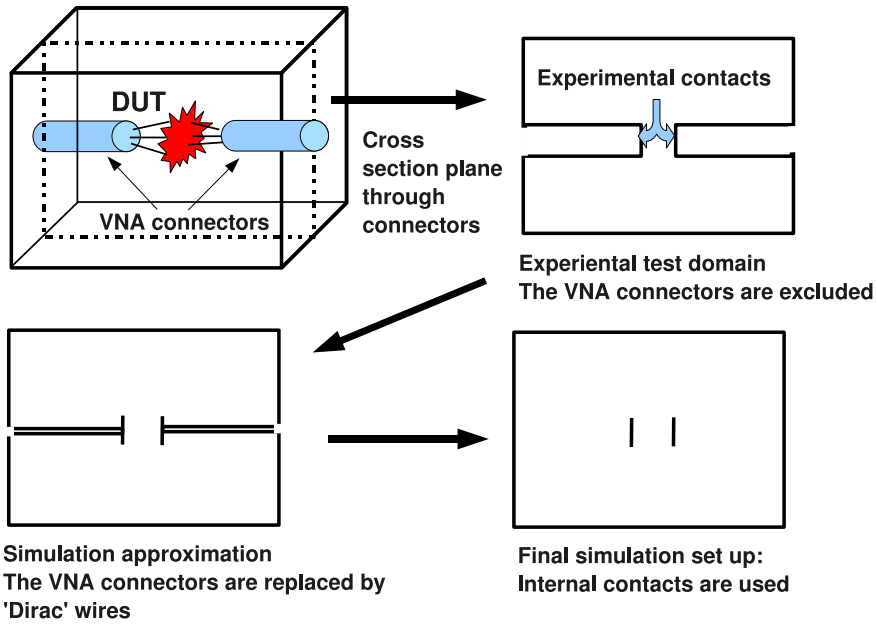

Figure 2: Illustration of the s-parameter measurement set up

- The voltage difference is given by the path-independent line integral of the electric field from the inner wire to the shield.

From these two observations, the computation of s-parameters can be done by loading ports with a given impedance and take one port for excitation. This is illustrated in Fig. 3.
As can be seen from Fig. 3, there will be a voltage value higher than zero at the "ground" contact at the port that is closed by the impedance Z_0. Indeed, the simulation of the device under test shows that at the contacts we find the following currents and voltages.

contact	voltage	current
s1	(1 , 0)	(-1.795945917651e-02 , 4.547205257826e-03)
s2	(8.612430634501e-01 , -2.768541083984e-01	1.724086402763e-02 , -5.792024534297e-03
g1	(0 , 0)	(-1.719576309564e-02 , 5.927621046340e-03)
g2	(3.810057208711e-03 , 8.892285617532e-03)	(-1.719576309564e-02 , 5.927621046340e-03)

As can be seen the voltage at the ground pad of the impedance differs from zero. The paradox arises if we want to link up this observation with the experimental set up. The question is: "What is correct voltage distribution along the closed loop of the two coax wire shields and the ground pads?" The answer is that the assumption of ideal grounds for this set up is not correct! As a consequence the result as given above is correct and the voltage at g2 is not equal to zero. There is a phase delay between the grounds g1 and g2. This delay is determined by the conductance of the metal in M1. A careful view inside this layer also reveals a current flow in opposite direction as the inductor. Therefore, the effective inductance appears less as what would expect for the static case. We found that the static inductance is 2.5 nH. For 1GHz we obtain without the use of Hodge operator modifications, an inductance of L=2.16 nH. Using the same set up for Neumann boundary conditions on the vector potential we find that L = 2.72 nH. Thus the test case clearly shows an impact on the inductance that compensates for an under-estimation with Dirichlet's boundary conditions.

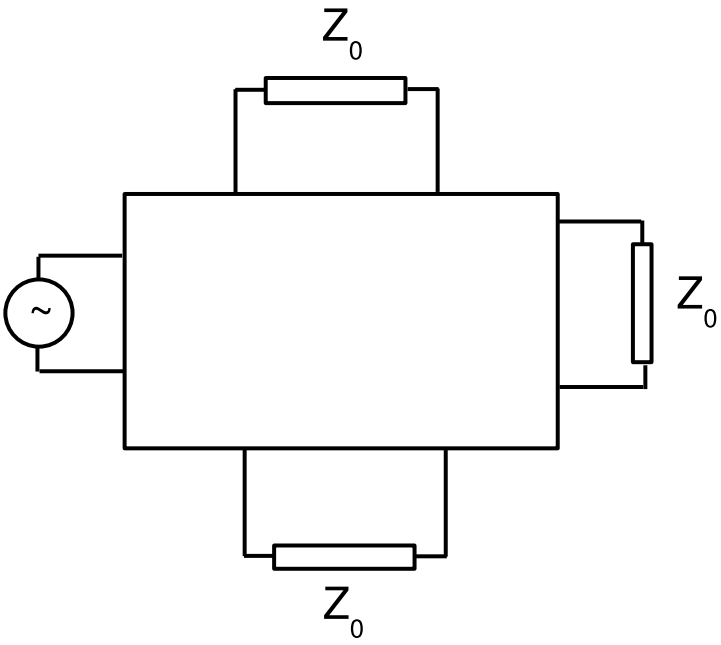

Figure 3: Illustration of the s-parameter measurement set up

One could think of defining static grounds being different from RF grounds as is common practice in compact modeling of RF devices. However, such an approach is not helping us here because the compact modeling of active devices does usually not include the magnetic sector and therefore, the static ground (operation point) can be safely decoupled from the RF ground. The same is true if the contacts are really located on the surface of the simulation domain. However, here we have argued that contacts may be internal.

5 Transient Development Software Test Structures

The transient solver has been developed using rather elementary test structures. Their purpose is in the first place to check whether the algorithms do the proper counting of degrees of freedom, mesh set up and contact allocation. Furthermore, the were used to achieve good communication between the solver and the GUI, as well as for building the post-processing facilities. The first structure consists of three layers of material of which the middle layer contains a semi-closed ring of metal. The structure is depicted in Fig. 4. The advantage of such a small structure is that one can manually count the number of nodes, number of links contact nodes et cetera. As a consequence, we know how much degrees of freedom this system generates. A next simple test structure includes one more layer. This layer is a conductive substrate. The substrate can be either semiconductor or insulator. The structure is shown in Fig. 5. Finally, we can modify the conducting ring by replacing the material with doped silicon.

6 Test of the Transient Solver on Large Inductors

In this chapter, we present the application of the transient solver to a large-scale inductor above a substrate. This structure was processed and characterized in the project CODESTAR (IST-2001-34058). The inductor has a square shape and consists of 4.5 windings. The CODESTAR project has produced numerous test structures which have been of vital importance for testing

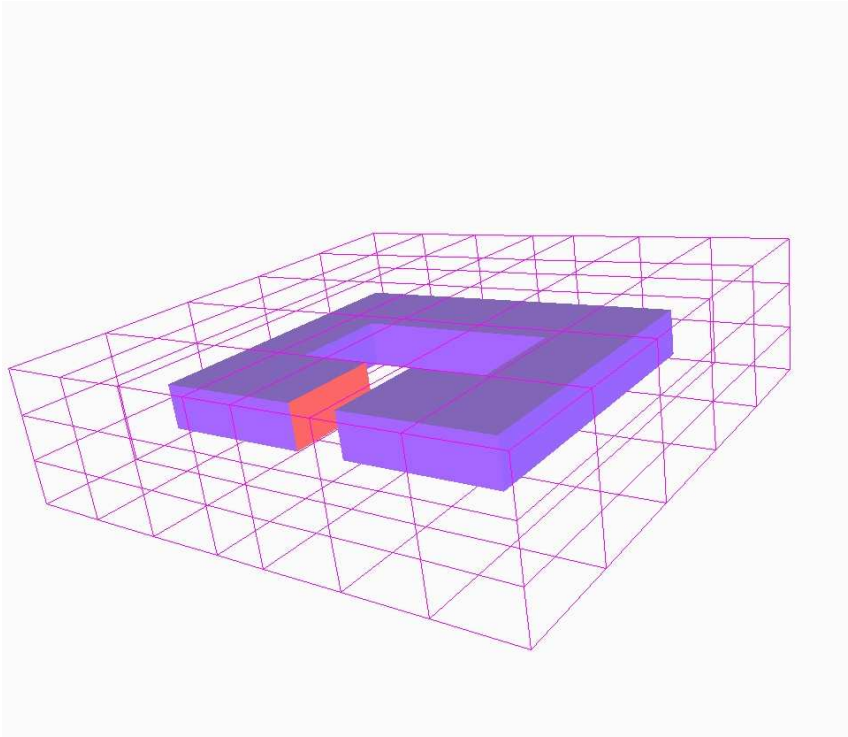

Figure 4: Simple test structure based in three layers of material with semi-closed loop inside

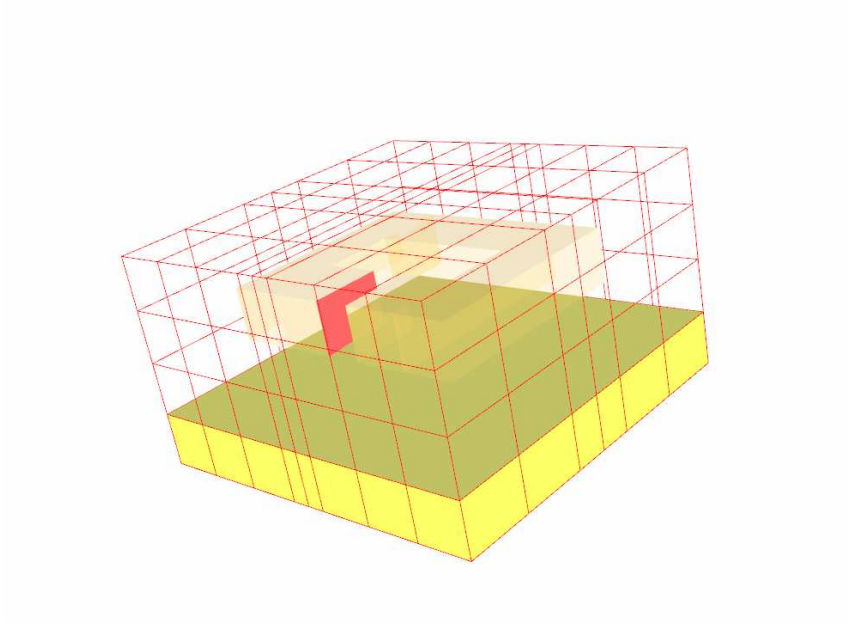

Figure 5: Simple test structure based in four layers of material with semi-closed loop inside

models and software implementation. The re-use of the CODESTAR results is an illustrative example of dissemination from one EU project into another. However, this time the analysis is performed in the transient regime. The layout of the structure is shown in Fig. 6. The result of the transient simulation is shown in Fig. 7 and Fig. 8. From these figures, we are able to read

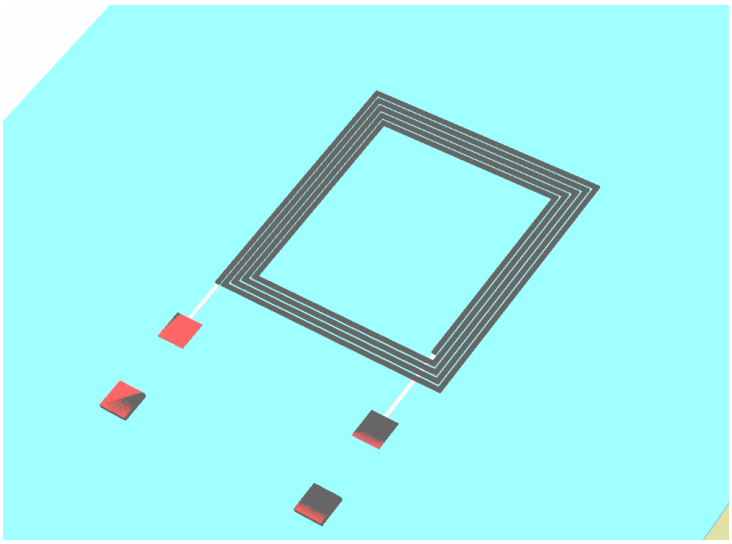

Figure 6: Lay-out of the 4.5 winding inductor above substrate.

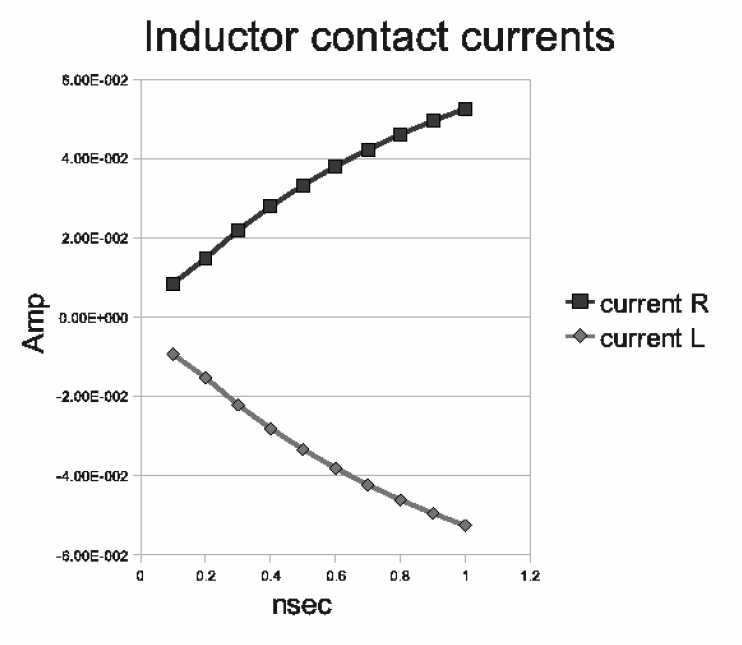

Figure 7: Result for the inductor current and substrate currents as a function of time.

off the inductance as well as the capacitive coupling to the substrate.

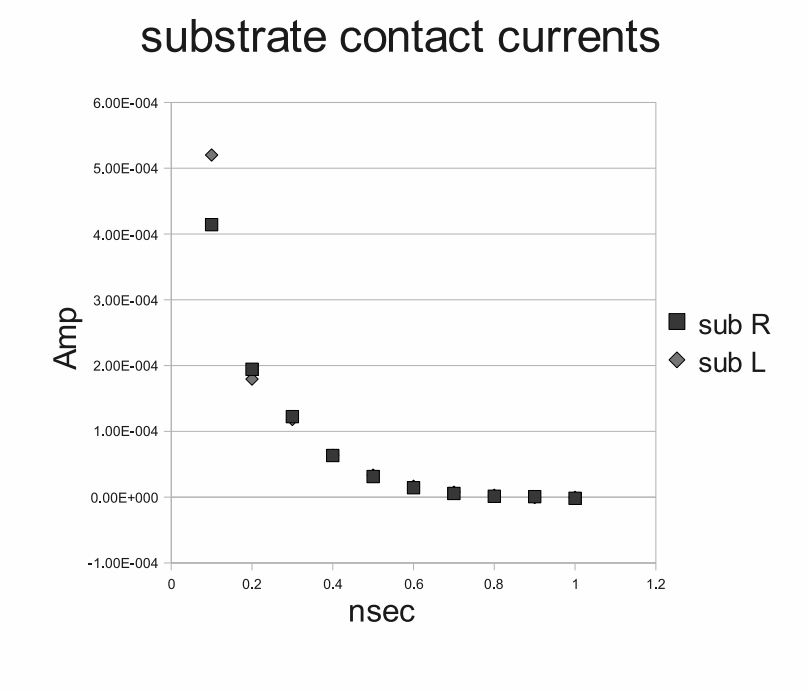

Figure 8: Result for the inductor current and substrate currents as a function of time.

7 Industrial Inductor Optimization

In this chapter we discuss the optimization and characterization of an inductor that is designed at NXP for building completely integrated systems on chip. Figure 9 illustrates the SoC. Linear modeling of oscillators does not provide accurate solutions and in most cases is not able to capture subtle nonlinear dynamics of oscillators (injection locking, jitter, etc). Therefore, nonlinear models are necessary which are fast, accurate and generic. Whereas, these models have been generated in the frequency domain, these modeling approaches are limited to small-signal characteristics. In the time domain we can access also there *large*-signal response. The inductor is designed for minimal substrate coupling by having opposite current circulations. The structure is shown in Fig. 10. In Figs. 11 and 12, three -dimensional screen shots of the inductor are shown.
The transient simulations have been performed from 0 to 1 nsec in 20 time steps. The results are shown below. In Fig. 13, the currents into and out of the inductor contacts are shown. Fig. 14 shows the logarithm of the inductor contact currents.

In Fig. 15, the current of the ground plane contact is shown in a logarithmic plot. Clearly, two time constants are observed.
The problem of lack of transient benchmark data is circumvented by starting from one of the benchmark cases and lift out a part that will be done with field solving in transient and another part will be evaluated using a circuit simulation approach. With his approach it is shown that a design flow can be put in place. MAGWEL and/or NXP demonstrated the design flow using an in-house inductor. The result of the simulation can be compared with a full lumped-element circuit simulation.

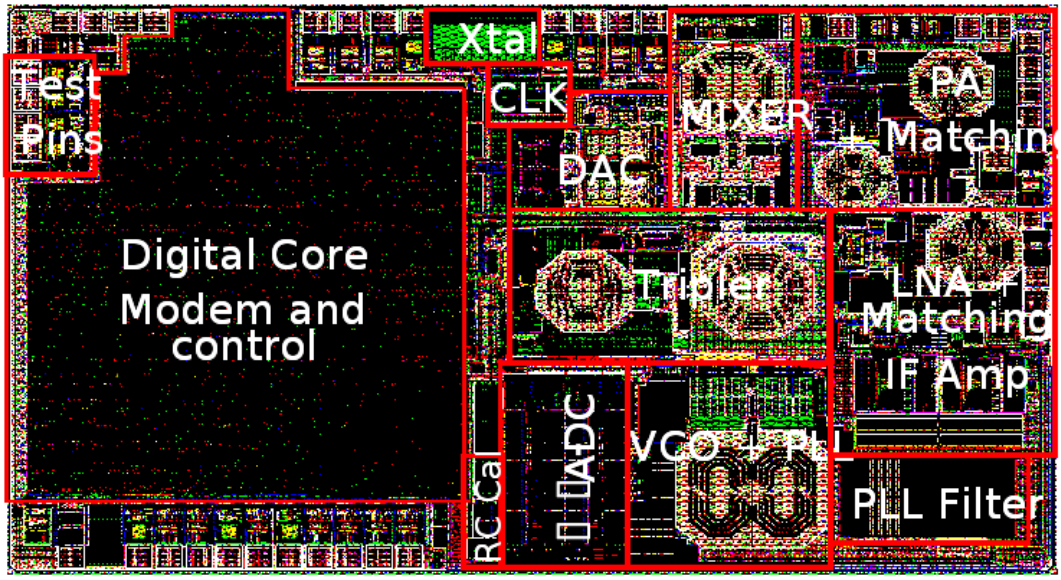

Figure 9: SoC with octo-shape inductor

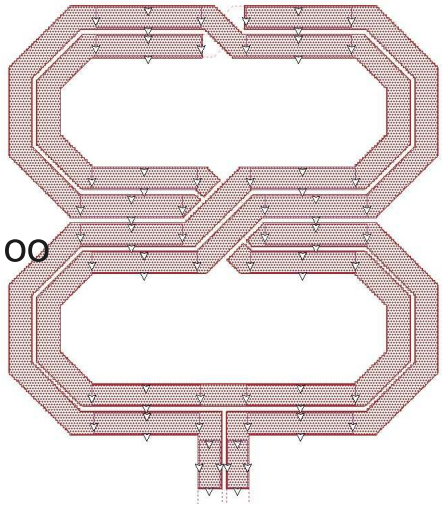

Figure 10: Inductor layout for optimized Q factors

In general the advantage of having a transient design flow in place is to circumvent the problems arising from using frequency domain EM models (S-parameters) in transient circuits. Often these S-parameter models turn out to have a lack of passivity and stability, resulting in transient solutions not converging, arising from failing to capture dominant poles in the right frequency plane. For this approach, as an example, the 8-shaped inductor can be used by comparing a

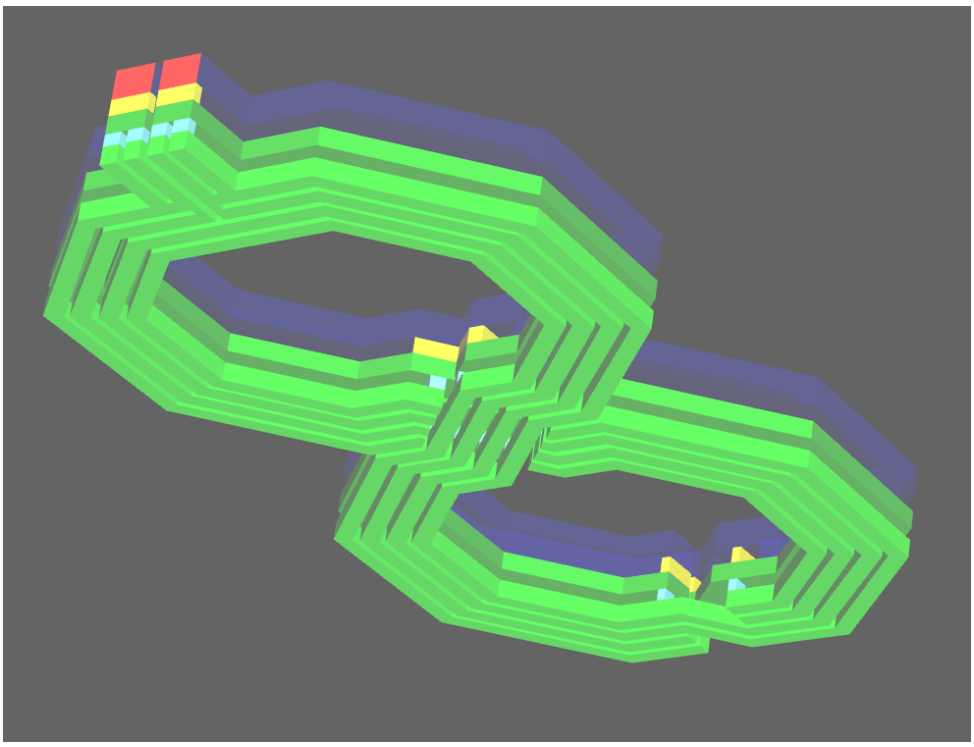

Figure 11: Inductor viewed from below

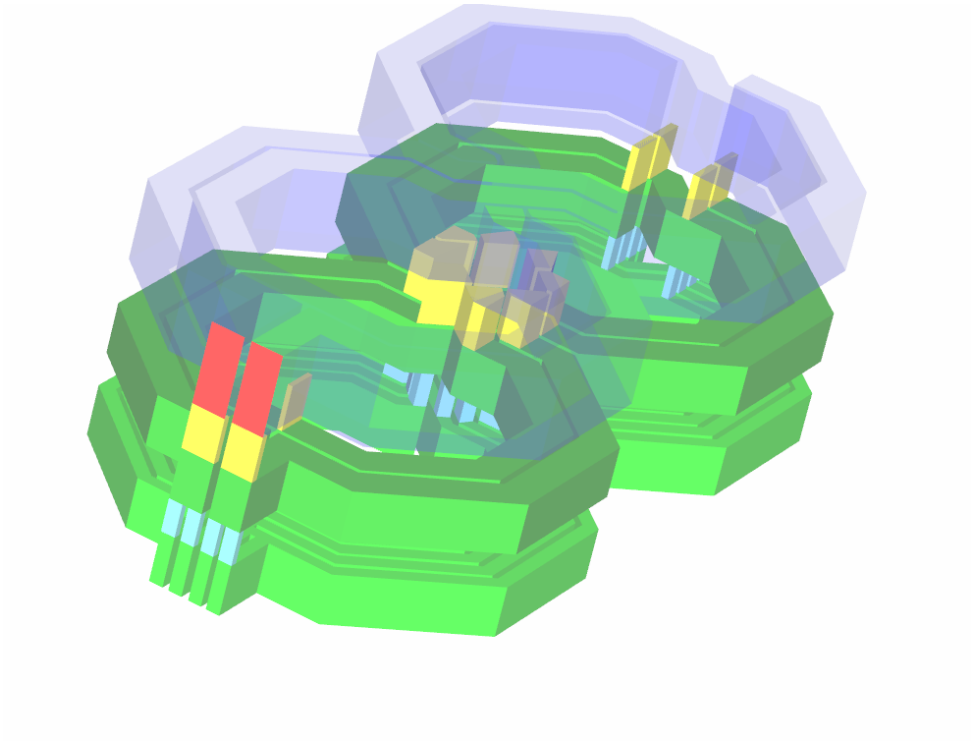

Figure 12: Inductor viewed from above with a stretched vertical coordinate

simple circuit with a simple lumped element inductor model in transient with the same circuit

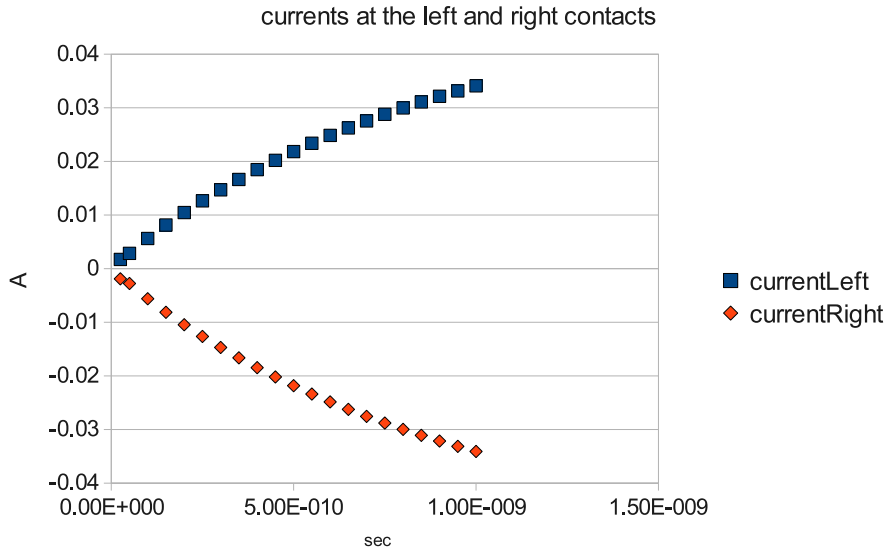

Figure 13: Value of currents at the left and right contact of the inductor

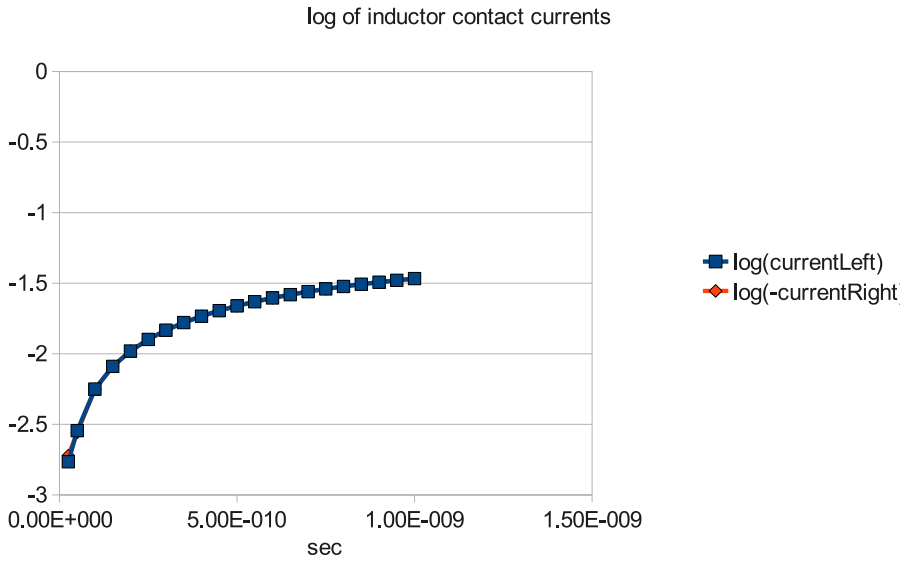

Figure 14: Logarithms of the (absolute) values of the inductor currents at the left and right contact.

coupled with the EM model.
In order to assess the results of the current build-up shown in Fig. 13, we represent the inductor as a simple lumped compact model (see Fig. 16), consisting of L, R and C to ground. As a first approximation we can take the values from the MAGWEL simulations, but in order to get a good fit, we took R=2 . Using a step magnitude of 1.0 Volt, the result in Fig. 17 is obtained. Applying a step magnitude of 0.1 Volt as was done for the field solver, we obtain the result of

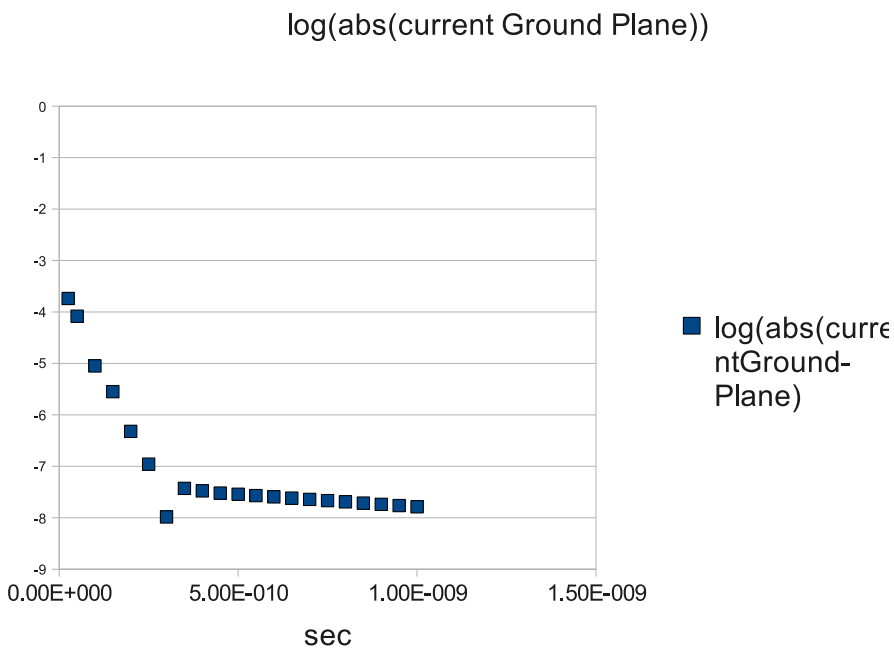

Figure 15: Logarithm of the absolute values of the current in the ground plane. Two time scales are observed.

Fig.18. The current build-up is shown to be in good agreement with the currents in Fig. 13.

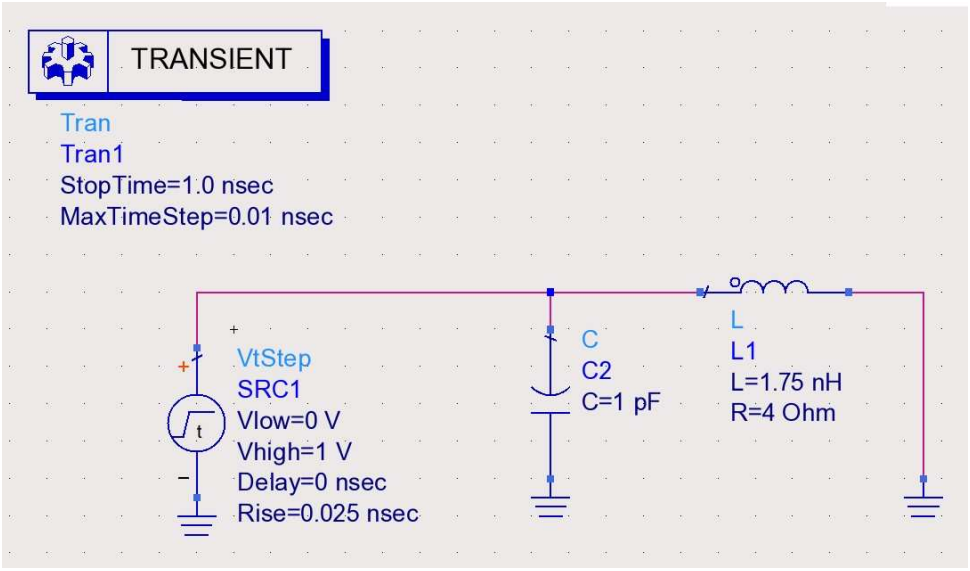

Figure 16: Set up of a compact model for the transient results.

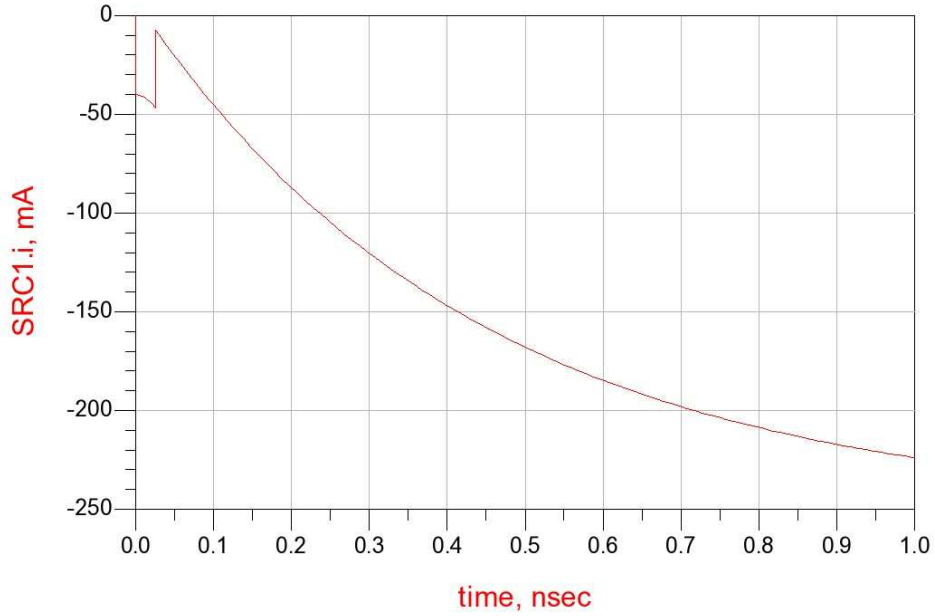

Figure 17: Results of a compact model for the transient simulation using 1V as step magnitude.

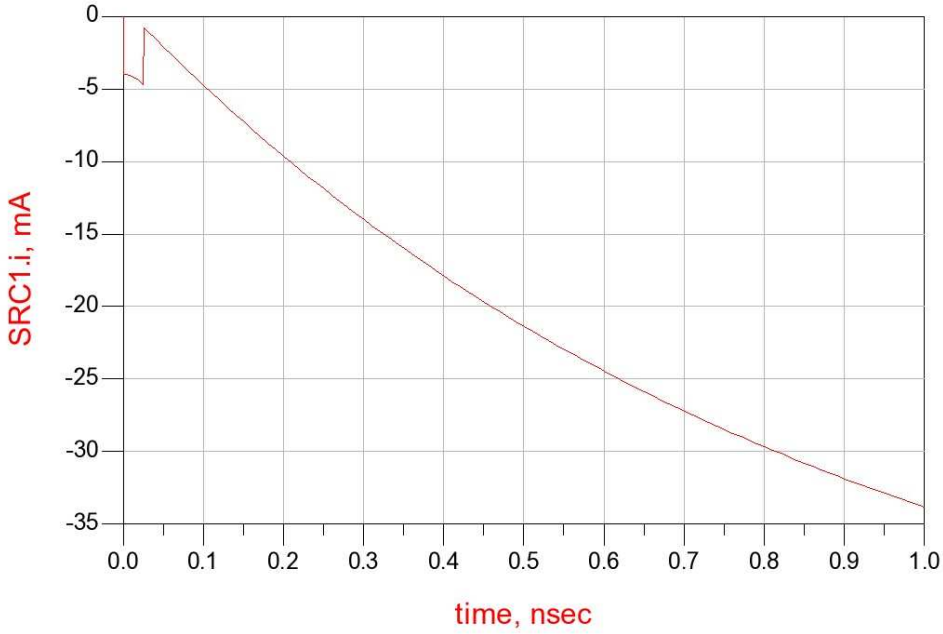

Figure 18: Results of a compact model for the transient simulation using a step magnitude of 0.1Volt.

8 Circuit examples

8.1 Ring Modulator

The Ring Modulator from figure 19 is a widely used benchmark circuit described in detail in [3] and `http://pitagora.dm.uniba.it/~testset/problems/ringmod.php` respectively. The

circuit mixes a low-frequent input signal U_{in1} with a high-frequent input signal U_{in2} producing a mixed signal in U_2. Depending on the artificial parasitic capacitance C_S we obtain a stiff

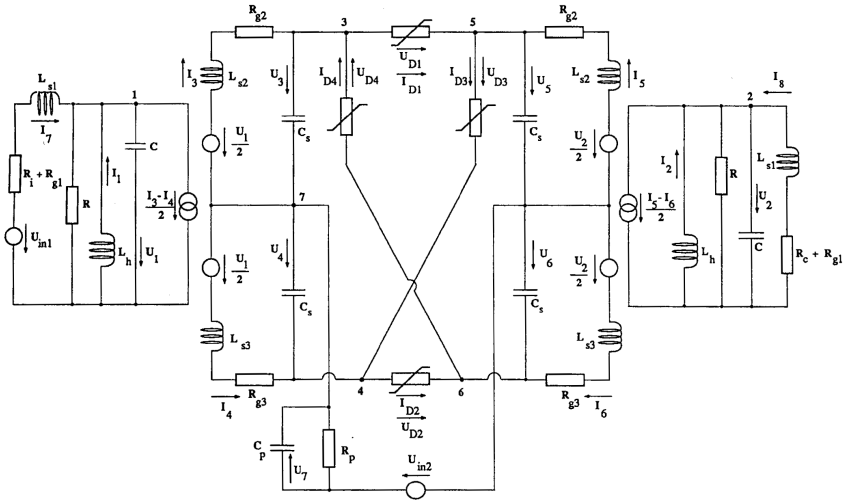

Figure 19: Circuit diagram for Ring Modulator taken from [3]

ordinary differential equation ($C_S \neq 0$) described by a system of 15 nonlinear equations or an index-2 differential-algebraic equation ($C_S = 0$) consisting of 11 differential and 4 algebraic equations. The artificial capacitance comes at the price of high frequent parasitic oscillations being introduced. For the modified nodal analysis the diodes are replaced by nonlinear resistors described by the voltage-current relation

$$I = g(U) = \gamma(e^{\delta U} - 1)$$

and the various constants of the model are given by

$$\begin{aligned} C &= 1.6 \cdot 10^{-8} & R &= 25000 \\ C_s &= 2 \cdot 10^{-12} & R_p &= 50 \\ C_p &= 10^{-8} & R_{g1} &= 36.3 \\ L_h &= 4.45 & R_{g2} &= 17.3 \\ L_{s1} &= 0.002 & R_{g3} &= 17.3 \\ L_{s2} &= 5 \cdot 10^{-4} & R_i &= 50 \\ L_{s3} &= 5 \cdot 10^{-4} & R_c &= 600 \\ \gamma &= 40.67286402 \cdot 10^{-9} & \delta &= 17.7493332 \end{aligned}$$

see [3]. The input signals are given by

$$\begin{aligned} U_{in1} &= 0.5 \sin(2000\pi t) \\ U_{in2} &= 2 \sin(20000\pi t) \end{aligned}$$

and the initial vales are chosen as zeros only. As the capacitors and inductors are linear, it is straightforward to formulate the equations in the form

$$A\frac{d}{dt}x + b(x,t) = 0$$

where A is a singular matrix in case of $C_S = 0$. Solving the Ring Modulator an $t = [0, 1 \cdot 10^{-3}]$ with model constants as above using DAEn [2] with the set of options

$$abstol = 10^{-4} \qquad reltol = 10^{-4}$$
$$estrat = 2$$

and we obtain the mixed signal U_2, see figure 20.

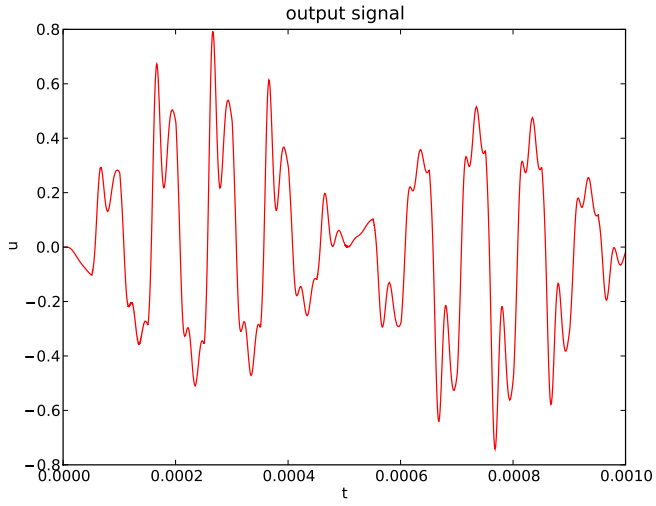

Figure 20: mixed low and high frequency output signal U_2 by the Ring Modulator

8.2 Oscillator

At first we briefly describe the models for MOSFETs implemented in MECS modeled by equivalent circuits. The MOSFETs in MECS are described by the following equations

$$\begin{aligned}
j_G - q'_{GD}(e_G - e_{Di}) + q'_{GS}(e_G - e_{Si}) &= 0,\\
j_S - \frac{e_S - e_{Si}}{Rs} &= 0,\\
j_D - \frac{e_D - e_{Di}}{Rd} &= 0,\\
-q'_{GD}(e_G - e_{Di}) + q'_{DB}(e_{Di} - e_B) - i_{BS}(e_B - e_{Di}) -&\\
\frac{e_D - e_{Di}}{Rd} + i_{DS}(e_{Di} - e_{Si}, e_G - e_{Si}, e_B - e_{Si}) + \frac{e_{Di} - e_{Si}}{Rsd} &= 0,\\
-q'_{GS}(e_G - e_{Si}) + q'_{SB}(e_{Si} - e_B) - i_{BS}(e_B - e_{Si}) -&\\
\frac{e_S - e_{Si}}{Rs} - i_{DS}(e_{Di} - e_{Si}, e_G - e_{Si}, e_B - e_{Si}) - \frac{e_{Di} - e_{Si}}{Rsd} &= 0.
\end{aligned}$$

Here the unknown functions are j_G, j_S, j_D (current through gate, source and drain contacts) and e_{Di}, e_{Si} (internal potentials). e_G, e_S, e_B and e_D are the potentials at gate, source, bulk and drain. Rs, Rd and Rsd are constants, see table 1. The functions q_{GD}, q_{GS}, q_{DB} and q_{SB} are

$$q_{SB}(u) = q_{DB}(u) = C_0 u, \;\; q_{GD}(u) = q_{GS}(u) = C_1 u,$$

Parameter name	Value in ME-MOSFET	Value in MD-MOSFET
Rsd	10^{15}	10^{15}
Rs	4	4
Rd	4	4
i_S	10^{-14}	10^{-14}
U_T	25.85	25.85
U_{T_0}	0.8	-2.43
β	$1.748 \cdot 10^{-3}$	$5.35 \cdot 10^{-4}$
γ	0	0.2
δ	0.02	0.02
Φ_0	1.01	1.28
Φ_B	0.87	0.87

Table 1: Sets of values for MOSFETs parameters

where C_0 and C_1 are also given constants, see table 1. The functions q_{SB} and q_{DB} can also be given as nonlinear functions of u as follows

$$q_{SB}(u) = q_{DB}(u) = \begin{cases} C_0\Phi_B\left(1 - \sqrt{1 - \frac{u}{\Phi_B}}\right), & u > 0, \\ C_0\left(1 + \frac{u}{4\Phi_B}\right)u, & \text{otherwise.} \end{cases}$$

where Φ_B is a constant. The function $i_{BS}(u)$ is as follows

$$i_{BS}(u) = \begin{cases} 0, & u > 0, \\ i_S\left(e^{u/U_T} - 1\right), & \text{otherwise.} \end{cases}$$

The values of i_S and U_T are also in table 1. The function $i_{DS}(u_{DS}, u_{GS}, u_{BS})$ is equal to

$$i_{DS}(u_{DS}, u_{GS}, u_{BS}) = \begin{cases} \beta u_{DS}\left(1 + \delta u_{DS}\right)\left(2(u_{GS} - U_T e(u_{BS})) - u_{DS}\right), & u_{GS} - U_T e(u_{BS}) > u_{DS}, \\ \beta\left(1 + \delta u_{DS}\right)\left(u_{GS} - U_T e(u_{BS})\right)^2, & u_{GS} - U_T e(u_{BS}) > 0, \\ 0, & \text{otherwise,} \end{cases}$$

if $u_{DS} > 0$. In case $u_{DS} = 0$ is $i_{DS}(u_{DS}, u_{GS}, u_{BS}) = 0$ and if $u_{DS} < 0$ the function is as follows

$$i_{DS}(u_{DS}, u_{GS}, u_{BS}) = \begin{cases} \beta u_{DS}\left(1 - \delta u_{DS}\right)\left(2(u_{GD} - U_T e(u_{BD})) + u_{DS}\right), & u_{GD} - U_T e(u_{BD}) > -u_{DS}, \\ -\beta\left(1 - \delta u_{DS}\right)\left(u_{GD} - UTe(u_{BD})\right)^2, & u_{GD} - U_T e(u_{BD}) > 0, \\ 0, & \text{otherwise,} \end{cases}$$

where $u_{BD} = u_{BS} - u_{DS}$, $u_{GD} = u_{GS} - u_{DS}$ and $U_T e(u) = U_{T_0} + \gamma\left(\sqrt{\Phi_0 - u} - \sqrt{\Phi_0}\right)$. The values of $\beta, \delta, U_{T_0}, \gamma, \Phi_0$ can also be found in table 1. The MOSFET characteristics with these two sets of parameters are shown in the Figures 21 and 22. The blue current corresponds to $u_{GS} = 1.0$. The current increases as u_{GS} increases. All MOSFETs are ME-MOSFETs. The first four MOSFETs have different contacts connected to the same circuit node. The following figures illustrate the behavior of the VCO.

Figures 23-24 show the transient response of the oscillator. The Figure 24 is just a zoom of Figure 23 around the tuning oscillation. The DAE solver DAEn was used to solve the resulting differential-algebraic equation with error strategy $estrat = 2$, absolute tolerance $atol = 10^{-6}$ and relative tolerance $rtol = 10^{-6}$.

The following is the net list of the oscillator simulated by MECS

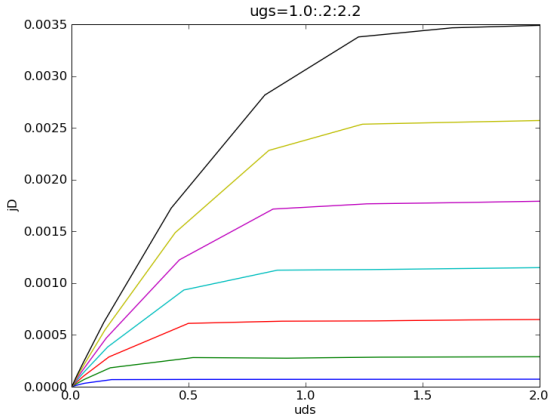

Figure 21: $u_{DS} - j_D$ characteristics for ME-MOSFETs

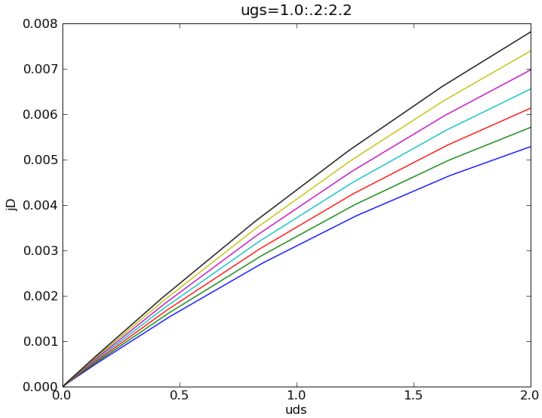

Figure 22: $u_{DS} - j_D$ characteristics for MD-MOSFETs

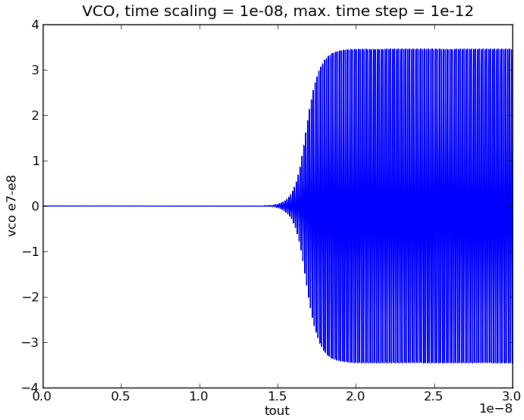

Figure 23: VCO transient response

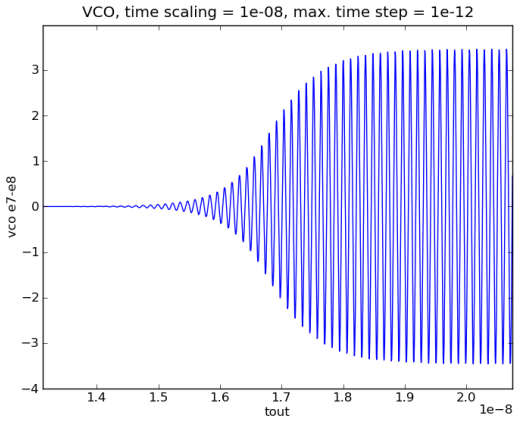

Figure 24: VCO transient response, zoom to smaller time interval around the tuning oscillation

```
* vco with level 2 mosfets
* five resistors
RmyR1 03 04 0.565e1
RmyR2 03 05 0.565e1
RmyR3 00 06 0.165e2
RmyR4 00 02 0.165e2
RmyR5 00 01 0.55e2

* six capacitors
CmyC1 02 08 0.46e-12
CmyC2 06 07 0.46e-12
CmyC3 07 08 0.3409e-12
CmyC4 01 03 0.1215e-11
CmyC5 08 00 0.5e-13
CmyC6 07 00 0.5e-13

* four inductors
LmyL1 04 07 0.65e-8
LmyL2 05 08 0.65e-8
LmyL3 03 14 0.1e-8
LmyL4 09 10 0.1e-8

* three voltage sources
VmyV1 14 00 2.0
VmyV2 09 00 0.0
VmyV3 09 13 0.0

* one current source
ImyI1 00 11 6.0e-3

* six mosfets, modeled by equivalent circuits
Mmymosfet1 11 11 10 10 mosfet0dME l=1.0 w=1.0
Mmymosfet2 13 08 13 10 mosfet0dME l=1.0 w=1.0
```

```
Mmymosfet3 13 07 13 10 mosfet0dME l=1.0 w=1.0
Mmymosfet4 10 11 12 10 mosfet0dME l=1.0 w=1.0
Mmymosfet5 08 07 12 10 mosfet0dME l=1.0 w=1.0
Mmymosfet6 12 08 07 10 mosfet0dME l=1.0 w=1.0

* mosfet model
.model mosfet0dME nmos (level=2 rs=4.0 rd=4.0 phi=1.01 kp=1.748e-3
+ vto=0.8 delta=0.02)
```

8.3 Coupled Circuit-Device Simulation

For the first fully coupled simulation with an direct, pointer based, communication between the MAGWEL solver for the electromagnetic field simulation and MECS for the circuit equation we consider a semi-closed loop of metal with two contacts, 144 metal nodes, 40 insulator nodes and 188 links as electromagnetic device, see figure 4. The circuit contains just two elements namely a simple sinusoidal source connected with the electromagnetic device model. The netlist reads

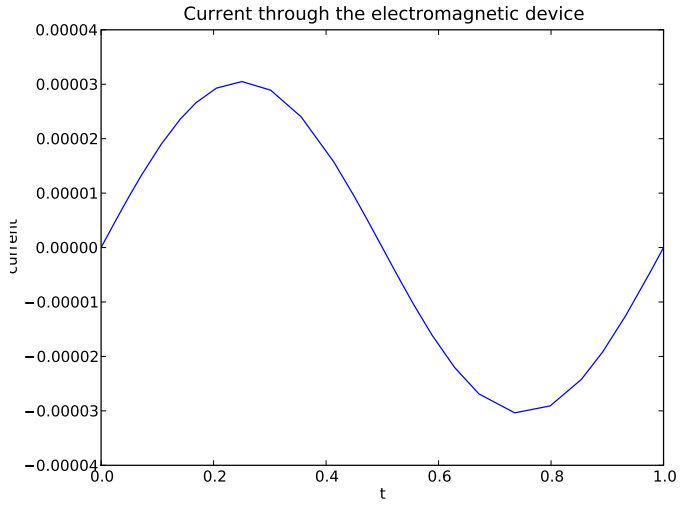

Figure 25: Current through the semi-closed loop

```
* Simple Circuit with one EM-Element, one voltage source and a resistor
V1 1 0 sin(0 1 1 0 0)
$EM1 1 0 simple_test.xml 1
```

where the $ implies a non-conform Spice3 element, see `http://bwrc.eecs.berkeley.edu/classes/icbook/spice/`. In more detail the line

```
$EM1 1 0 simple_test.xml 1
```

implies that the electromagnetic device is located between node 1 and 0, is modeled by the MAGWEL xml structure `simple_test.xml` and the 1 say which contact is the reference contact for the current calculation. Figure 25 show the current through the electromagnetic device. DAEn was used to solve the resulting differential-algebraic equation with the standard options.

In general the equations for the coupled circuit-device simulation read

$$\begin{aligned}
A_C q' + A_R g(A_R^T e, t) + A_L j_L + A_M j_M + A_V j_V + A_I i_s(t) &= 0 \\
q - q(A_C^T e, t) &= 0 \\
\phi' - A_L^T e &= 0 \\
\phi - \phi(j_L, t) &= 0 \\
A_V^T e - v_s(t) &= 0 \\
A_{00}\mathcal{V} + A_{10}\frac{\mathrm{d}}{\mathrm{d}t}\mathcal{V} + \mathcal{A}_{11}\Pi + A_{21}\frac{\mathrm{d}}{\mathrm{d}t}\Pi + B_{00}hA_M^T e + B_{10}hA_M^T\frac{\mathrm{d}}{\mathrm{d}t}e &= 0 \\
\Pi - \frac{\mathrm{d}}{\mathrm{d}t}\mathcal{A} &= 0 \\
A_{02}\mathcal{V} + A_{03}\mathcal{A} + A_{12}\frac{\mathrm{d}}{\mathrm{d}t}\mathcal{V} + A_{13}\Pi + A_{23}\frac{\mathrm{d}}{\mathrm{d}t}\Pi + B_{01}hA_M^T e + B_{11}hA_M^T\frac{\mathrm{d}}{\mathrm{d}t}e &= 0 \\
C_{00}\mathcal{V} + C_{10}\frac{\mathrm{d}}{\mathrm{d}t}\mathcal{V} + C_{11}\Pi + C_{21}\frac{\mathrm{d}}{\mathrm{d}t}\Pi + D_0 hA_M^T e + D_1 hA_M^T\frac{\mathrm{d}}{\mathrm{d}t}e + Lj_M &= 0
\end{aligned}$$

with solution $x = (e,\ \phi,\ j_L,\ q,\ j_V,\ \mathcal{V},\ \mathcal{A},\ \Pi,\ j_M)$ and

$$A_i = \begin{bmatrix} A_{i0} & A_{i1} \\ A_{i2} & A_{i3} \end{bmatrix},\ C_i = \begin{bmatrix} C_{i0} & C_{i1} \end{bmatrix},\ i \in \{0,1,2\},\ B_i = \begin{bmatrix} B_{i0} \\ B_{i1} \end{bmatrix},\ i \in \{0,1\}\ .$$

The system can be formulated as a differential-algebraic equation of the form

$$A\frac{d}{dt}x + b(x,t) = 0.$$

The stand-alone equations for the electromagnetic device can be formulated as

$$\begin{aligned}
A_0\begin{pmatrix}\mathcal{V}\\ \mathcal{A}\end{pmatrix} + A_1\frac{\mathrm{d}}{\mathrm{d}t}\begin{pmatrix}\mathcal{V}\\ \mathcal{A}\end{pmatrix} + A_2\frac{\mathrm{d}^2}{\mathrm{d}t^2}\begin{pmatrix}\mathcal{V}\\ \mathcal{A}\end{pmatrix} + B_0 U + B_1\frac{\mathrm{d}}{\mathrm{d}t}U &= 0 \\
C_0\begin{pmatrix}\mathcal{V}\\ \mathcal{A}\end{pmatrix} + C_1\frac{\mathrm{d}}{\mathrm{d}t}\begin{pmatrix}\mathcal{V}\\ \mathcal{A}\end{pmatrix} + C_2\frac{\mathrm{d}^2}{\mathrm{d}t^2}\begin{pmatrix}\mathcal{V}\\ \mathcal{A}\end{pmatrix} + D_0 U + D_1\frac{\mathrm{d}}{\mathrm{d}t}U + Y &= 0
\end{aligned}$$

whereas $U = hA_M^T e$ is the applied voltage at the contacts where h is the auxiliary functions and $Y = Lj_M$ is the current through the electromagnetic device. The discretization of Maxwell's equations in space lead to an linear differential-algebraic equation.

9 Test of the linear MAGWEL-MECS interface

We need as input for MECS in the initial step:

- Number of nodes
- Number of links
- Number of contacts
- Flag: semiconductor {True/False}
- In case of no semiconductor being present: The matrices A, B, C and D, more precisely: $A_0, A_1, A_2, B_0, B_1, C_0, C_1, C_2, D_0, D_1$.

We need the number of links, nodes and contacts for the right shape of our matrices and to split them, see below. All matrices are in the matrix-market format, i.e. a series of row-column-value lines. Remember as well that we do the substitution of $dA/dt = \Pi$ in the linear case, i.e. we need 10 matrices.

10 Linear Coupling

The linear coupling is exploits the state-space description approach and at the same time uses the fact that a differentiation to time corresponds to a factor $\exp \imath\omega t$ in the frequency domain. The state-space description is:

$$\begin{bmatrix} \mathbf{A} & \mathbf{B} \\ \mathbf{C} & \mathbf{D} \end{bmatrix} \cdot \begin{bmatrix} \mathbf{X} \\ \mathbf{U} \end{bmatrix} + \begin{bmatrix} \mathbf{0} \\ \mathbf{Y} \end{bmatrix} = 0 \tag{1}$$

The **A** - matrix takes the following form

$$\mathbf{A} = \mathbf{A}_0 + \mathbf{A}_1 \frac{\mathrm{d}}{\mathrm{d}t} \tag{2}$$

end similar expressions for $\mathbf{B}, \mathbf{C}, \mathbf{D}$. The linear interface is based on exchanging the matrices A,B,C,D We designed the interface such that MEC needs as an input 10 matrices . This gives MECS the control to substitute $\frac{\mathtt{d}}{\mathtt{d}t}A = \Pi$ and this work is already done. As this completely specifies the transient operation it makes sense to leave it to MECS. All that is needed is to provide these 10 matrices $A_0, A_1, A_2, B_0, B_1, C_0, C_1, C_2, D_0, D_1$. So all that was needed to be done is to get MECS and MAGWEL communicate once to exchange the matrices by pointers.

11 Nonlinear Coupling

The Modified Nodal Analysis leads to a DAE of the following type.

$$A\frac{\mathtt{d}}{\mathtt{d}t}d(x,t) + b(x,t) = 0$$

where A is a constant matrix and d and b are functions depending on $x = (e, j_V, j_L)$ and the time t. The EM system can be split into two vector valued equations, one corresponding to the Maxwell system (i.e. the discretized Gauss equation and the discretized Maxwell-Ampere equation) and one to the discretized current equation. In the linear case this was the same with the matrices A, B, C, D. In the nonlinear case we would write these two equations in the following way:

$$\tilde{A}\frac{\mathtt{d}}{\mathtt{d}t}\tilde{d}(x,t) + \tilde{b}(x,t) = 0 \tag{3}$$

$$\hat{A}\frac{\mathtt{d}}{\mathtt{d}t}\hat{d}(x,t) + \hat{b}(x,t) = Y \tag{4}$$

Here $x = (V, n, p, A, \Pi, V_{app})$ and Y is the current through the contacts.
Experience in transient simulations has learned that the discretization of $\frac{\partial}{\partial t}(\phi_i^p - V_i)$ induces loss of charge conservation, therefore, we will apply the BDF rules on $\mathrm{e}^{(\phi_i^p - V_i)}$. If we put everything in the n, p notation we get here:

$$\Delta w_i \, \frac{1}{p_i} \, \frac{\partial}{\partial t} p_i + \sum_j \, \mu_p \frac{d_{ij}}{h_{ij}} \left(B[X_{ij}] - \frac{p_j}{p_i} B[-X_{ij}] \right) + \frac{R(p_i, n_i)}{p_i} \, \Delta w_i = 0$$

We see here that the part in front of the time derivative is not constant anymore. This leads to $\tilde{A}$ not being constant. The fact that we can write

$$\frac{1}{p_i}\frac{\partial}{\partial t} p_i \quad \text{or} \quad \frac{\partial}{\partial t} ln(p_i)$$

is indeed an important question. Considering the non constant term in front of the time derivative leads to a different formulation of the equations altogether (being a more general one.

For electrons we have

$$\Delta w_i \, \frac{1}{\mathrm{e}^{(V_i-\phi_i^n)}} \, \frac{\partial}{\partial t}\mathrm{e}^{(V_i-\phi_i^n)} + \sum_j \mu_p \frac{d_{ij}}{h_{ij}} \left(B[-X_{ij}] - \frac{n_j}{n_i} B[X_{ij}] \right) + \frac{R(p_i, n_i)}{n_i} \, \Delta w_i = 0 \qquad (5)$$

From the discussion above, it is clear that the communication between the MNA and the EM solver, is effected by the scaling procedure. Fortunately, this is not a show stopper.
At each time instant we can extract from the EM solver the matrices

$$\tilde{A} = \Delta w_i \, \delta_{lm} \qquad (6)$$

where δ_{lk} is the identity (unit) matrix. Since the state - space variables V, ϕ^p, ϕ^n are known at any instant both in the EM solver and by pointers accessible by the DAEn solver, a conversion to p and n can be done 'on-the-fly'. The ME solver assembles the remainder term $\tilde{b}$ using the state-space content and the geometrical situation.

11.1 Technical realization

Figure 26 gives a good overview of the whole coupling idea between the MECS solver and the EM solver.

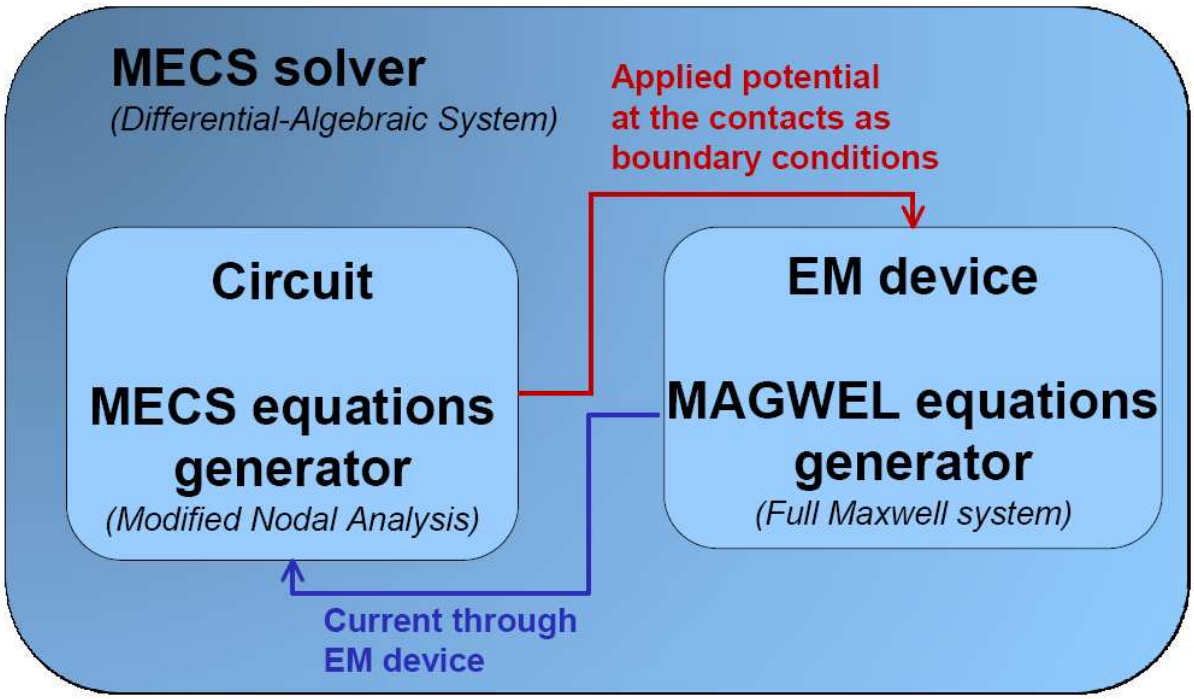

Figure 26: Coupling MECS solver with EM.

On the technical level one has to specify how the the two software packages interact (figure 27). Since the MECS solver is written in Python and the EM solver in C/C++ we use Cython as a communication bridge, cf. `http://cython.org/`. Cython is a programming language which understands both C/C++ code and Python code and it is possible to exchange data types. The data exchange is realized via pointers to vectors and matrices. The EM solver functionality is available via a shared library.

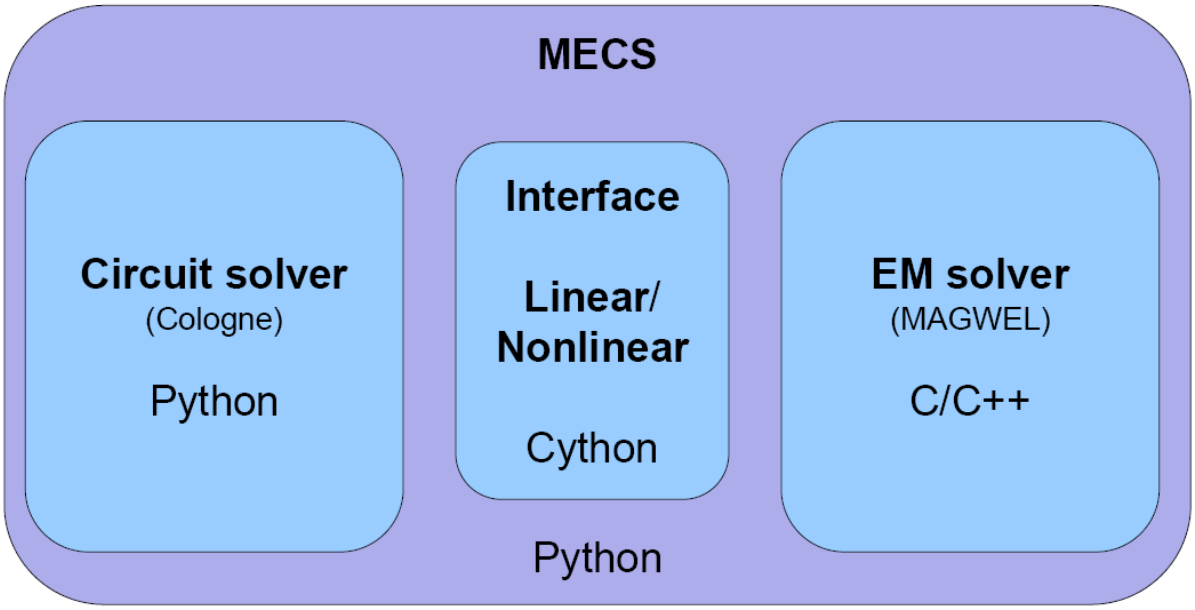

Figure 27: Technical coupling MECS solver with EM via Cython.

In the following we will highlight the calling order of the nonlinear interface a little bit more.

- The first step is that MECS starts the EM solver via the function

```
char** magwel_nonlinear_init(char *model){
  constructSolvEMAPI( model );

  int nrLinks = getNrLinks();
  int nrNodes = getNrNodes();
  int nrSemiconductorNodes = getNrSemiconductorNodes();
  int nrContacts = getNrContacts();
  int sizeV = getSizeV();
  int sizeP = getSizeP();
  int sizeN = getSizeN();
  int sizeA = getSizeA();
  int sizePi = getSizePi();
  int sizeVappl = getSizeVappl();
  ...
  return init_array_pointers;
  }
```

  It constructs the API for the EM solver and as init information returns the number of nodes, links, etc. This information is needed to construct the matrices in the MECS solver with the right dimensions.

- Running through the time integrator an update for a new input at a new time point is needed. So the matrices $\tilde{A}$, $\hat{A}$, $\tilde{b}$, $\hat{b}$ need to be extracted from the EM part. This is done with the function

```
char** magwel_nonlinear_update(char *model, double *input_V,
  double *input_p,double *input_n,
  double *input_A,double *input_Pi,
  double *input_Vapp){
  ...
  loadStateVariables( input_array_pointers );

  computeStateSpace();

  constantPartEM_matrix = getConstantPartEM();

  staticPartMaxwellEM_array = getDiscretizedStaticMaxwellEM();
  staticPartCurrentEM_array = getDiscretizedStaticCurrentEM();

  confirmResultsRead();
  ...
  return output_array_pointers;
  }
```

First the state variables (x) are loaded into the EM solver and then the full Maxwell system is solved (computeStateSpace()). The output is then extracted in form of $\tilde{A}$, $\hat{A}$, $\tilde{b}$, $\hat{b}$.

- The nonlinear interface also provides a stopping function which shuts down the EM solver because it is not needed anymore. It takes care of memory deallocation in the EM solver part.

```
void magwel_nonlinear_stop(){

  deallocateStateMatrices();

  destroySolvEMAPI();

  return;
  }
```

The linear interface works about the same. The main difference here is that we exchange only matrices and that we need to call the update function only once.

11.2 Scaling choices

Scaling is a major issue in the technical debugging process. In order to clarify the situation here we present a short overview of scaling choices for a Differential-Algebraic Equation. We distinguish between three types of scaling:

- Scaling of variables
- Scaling of time
- Scaling of equations

We start with the completely unscaled equation

$$A(x_u(t_u))\frac{d}{dt_u}x_u(t_u) + b(x_u(t_u)) = 0$$

for the unscaled input x_u at the unscaled time t_u. Now introducing the variable scaling

$$Sx_s = x_u$$

where S is a diagonal matrix which is fixed for all times we get equivalently

$$A(Sx_s(t_u))\frac{d}{dt_u}\left(Sx_s(t_u)\right) + b(Sx_s(t_u)) = 0.$$

Now we put the time scaling into play via

$$t_s = \alpha t_u$$

with the scaling factor α. Defining

$$\tilde{x}_s(t_s) := x_s(\alpha t_s)$$

and using that

$$\frac{d}{dt_u}\left(x_s(t_u)\right) = \frac{d\tilde{x}_s}{dt_s}\frac{dt_s}{dt_u} = \alpha\frac{d\tilde{x}_s}{dt_s}$$

we get

$$\alpha A(S\tilde{x}_s(t_s))S\frac{d}{dt_s}\left(\tilde{x}_s(t_s)\right) + b(S\tilde{x}_s(t_s)) = 0.$$

which is then the scaled equation. Notice that we did not use scaling of equations here which is basically multiplying every row by a specific factor which is independent of time and the variables. We assume here that this is already done when producing A and b.

12 Conclusion

Workpackage 3 of ICESTARS has focused on three main subjects for providing field solving support for RF circuit simulation.

- First of all, complementary to frequency simulation which is based on small-signal analysis, a transient field solver was developed. Although transient field solvers are already available in some form (CST, HFSS) , the underlying field solver exploits the potential formulation which is a necessity when semiconducting materials are involved. The potential formulation requires specific care in order to arrive at a well-posed set of equations. With the benchmarks that have been simulated, we have shown that the novelties that were introduced have resulted into a problem formulation that is indeed solvable by standard numerical techniques. We have 'proved' the correctness of the problem set up by demonstrating computational evidence. Of course, this is not a mathematically satisfactory proof, but for the time being such a general proof is lacking and at least we can claim that the proposed formulation makes sense.

- A second major theme of work in WP3 has been to set up a 'holistic' co-simulation. The underlying idea is that circuits and fields each provide their own set of differential algebraic equations, and when correctly 'glued' together, i.e. giving a consistent and complete set of cross couplings, the newly assembled system is solvable.

- Finally the third objective of the effort in WP3 was to support the tool development by applications to industrial-relevant cases and to arrive at a set of test cases serving as reference benchmarks. A series of cases have been presented both in D3.1 and the underlying deliverable. The effort not only dealt with spatial discretization but also with time integration in circuit simulations and adaptive time stepping algorithms. The latter techniques have also been applied to highly non-trivial cases as was shown in section 8.

Despite these three achievements, not all goals within WP3 have been reached. A major obstacle has been the availability of test cases on transient measurements. In particular, for on-chip devices, we did not get access to data which were gathered as transient responses. Therefore, a work around needed to be developed to test the quality of the solutions. This was done by comparing the results of extracted compact models with the results from S-parameter measurements.

References

[1] Wim Schoenmaker, Peter Meuris, Walter Pflanzl and Alexander Steinmayr: *Evaluation of Electromagnetic Coupling Between Microlectronic Device Structures Using Computational Electrodynamics* Invite presentation at the Conference on Scientific Computing in Electrical Engineering SCEE 2008, Helsinki Finland, Eds. Janne Roos Luis R.J. Costa, published in the series Mathematics in Industry vol. 14 , Springer Verlag Berlin Heidelberg

[2] M. Hanke: *A New Implementation of a BDF method Within the Method of Lines*, Report No. 2001:01, Royal Institute of Technology, Stockholm, 2001.

[3] F. Mazzia and F. Iavernaro. *Test Set for Initial Value Problem Solvers, release 2.4.* Department of Mathematics, University of Bari, 2006. `http://pitagora.dm.uniba.it/~testset/`